Chapter V

Adsorption using Treated Elaeocarpus tectorius seeds (TETS)

Chapter V

Adsorption using Treated *Elaeocarpus tectorius* Seeds (TETS)

Efficacy of treated *Elaeocarpus tectorius* seed (TETS) in sequestrating PO_4^{3-}, NO_3^- and SO_4^{2-} anions from aqueous matrices by batch mode is dealt in this chapter.

5.1 Microscopic Analysis

Optical microscopic images of natant and treated counterparts of the sample (0.18 mm particle size) are picturized in figures 5.1a and b. Greater porosity exhibited by TETS is obvious, confirming the effective chemical modification.

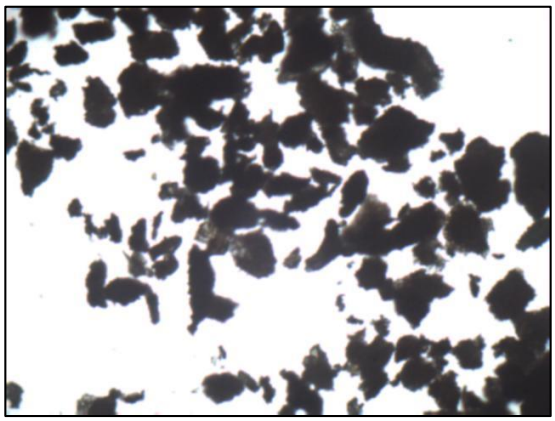

Figure 5.1a Raw ETS

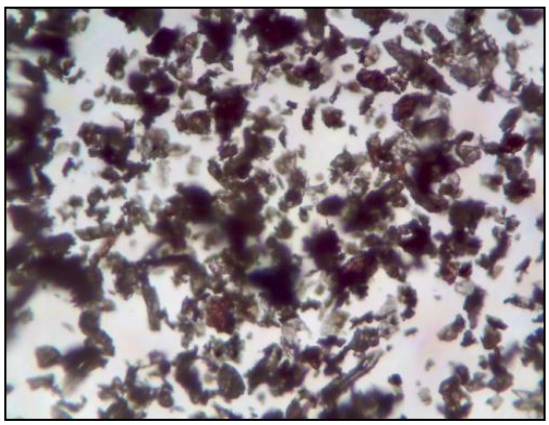

Figure 5.1b Treated ETS

5.2 Physio- Chemical Characterization

Parametric values of physiochemical characteristic studies of TETS are listed in Table 5.1.

Table 5.1 Physio- Chemical Characteristics

Properties	TETS (0.18 mm)
pH	7.2
Conductivity(mV)	38.73
Moisture (%)	0.87
Bulk density (g/L)	0.63
Specific gravity	1.35
Porosity	51.58
Ash content (%)	2.04
Acid Soluble Matter (%)	2.12
Water Soluble Matter (%)	3.46
Ion Exchange Capacity (m_{eq} /g)	0.37
pH_{zpc}	6.90
Surface area (m^2/g)	58.63
Mean Pore diameter (nm)	2.30
Carbon (%)	48.91
Nitrogen (%)	2.67
Hydrogen (%)	7.69
Sulphur (%)	0.52
Surface Acidic groups (m $molg^{-1}$)	
Phenolic	0.34
Carboxylic	1.48
Lactonic	0.13

Neutral pH/ pH_{zpc} values imply the possibility of anion sorption without any ionic interference. Lower moisture content defines less agglomeration, surface group dissociating property of TETS material[1]. Ash content value (≈ 2%) exhibits enhanced sorption of the material with abundant carbon content (48.91%), indicative of extended active sites. Specific gravity/bulk density values being > 2 favours down flow operation,

supported by fine particles of greater pore volume. Surface area (58.63 m^2/ g) and mean pore diameter (2.3 nm) calculated from BET/ BJH plots (figs 5.2 & 5.3), imply mesoporous nature of TETS[2]. Water/ acid soluble matter being > 5 %, ensure insoluble nature, thereby aiding its use in the acidic/ basic environments.

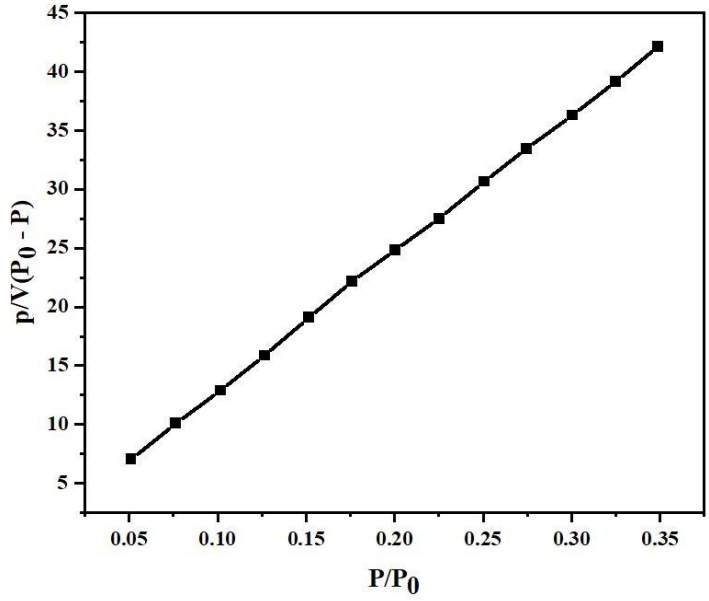

Figure 5.2 BET Plot

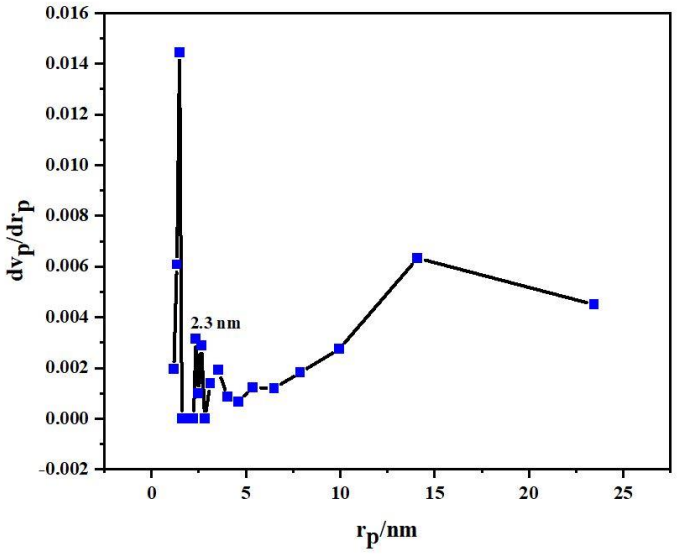

Figure 5.3 BJH Plot

Recondense of type IV hysteresis loop pattern[3] is evident from figure 5.4, the adsorption – desorption isothermal plot, being similar to that obtained for TCSS material (in chapter IV).

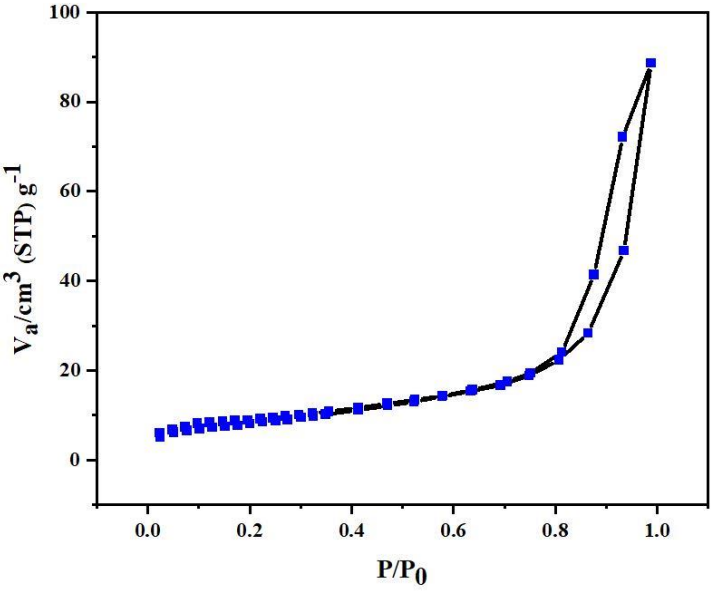

Figure 5.4 Adsorption / Desorption Isothermal Plot

Certain physiochemical properties of TETS were compared with the specific values reported for other sorbent materials. Tabulated data shows that the fruit seeds employed in this study exhibited minimal values of ash content, bulk density and moisture content, with marked surface-active sites against other materials.

Table 5.2 Materials Characteristics vs Literature Report – A Comparison

Adsorbents	Ash Content (%)	Bulk Density (g/L)	Moisture Content (%)
Jatropha curcas fruit shell[4]	5.87	9.95	0.45
Adonsonia digitata fruit shells[5]	7.29	2.81	0.44
Barassus aethiopum seed[6]	9.20	4.10	0.33
Mango seed[7]	2.33	15.47	26.79
Cashew nut shell[8]	2.75	9.83	65.4
Eleoacarpus tectorius fruit seed (current study)	**2.04**	**0.63**	**0.87**

5.3 SEM and EDAX Analyses

SEM micrographs of natant, treated and anion loaded TETS are illustrated in figures 5.5- 5.9. Figure 5.6 depicts the availability of many surface voids[9] against its native precursor (fig 5.5). This shows that removal of lignin, hemicellulose and other extractives from fruit seeds might have occurred during acid treatment[10]. The visible open pores of TETS have been covered and blocked by the anions during sorption, which is evident from the smooth surface morphologies. (figs 5.7 – 5.9)

EDAX spectra of unloaded TETS and sorbate laden counterparts are presented in figures 5.10 - 5.13. Uptake of anions by TETS and their relevant peaks can be referred from the specified spectral lines.

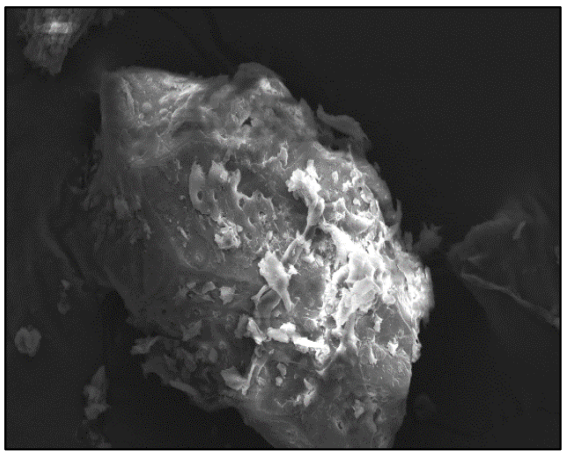

Figure 5.5 Raw ETS

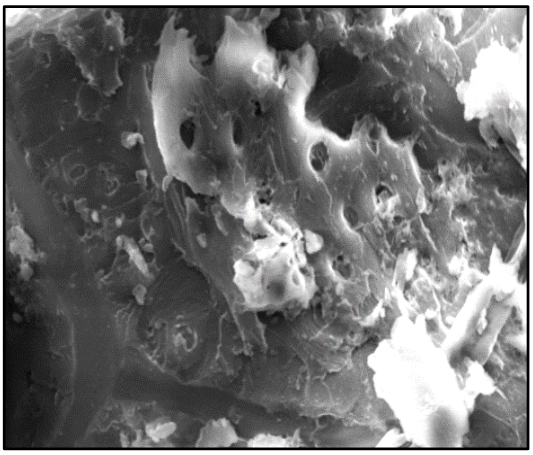

Figure 5.6 Treated ETS

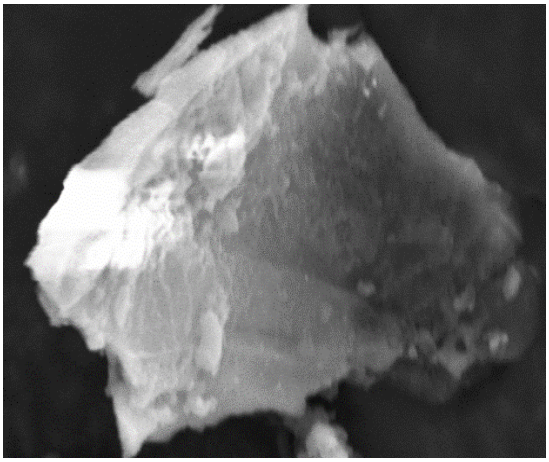

Figure 5.7 PO_4^{3-} loaded TETS

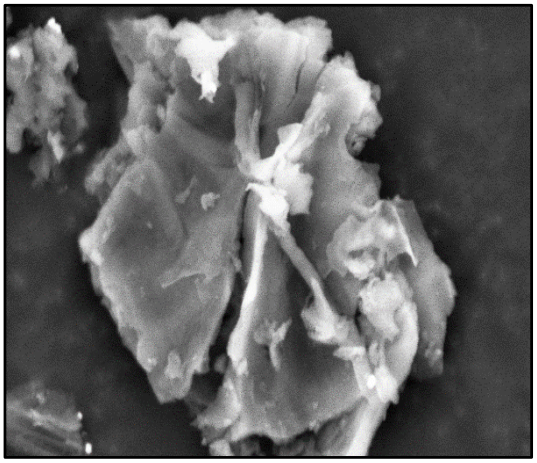

Figure 5.8 NO_3^- - loaded TETS

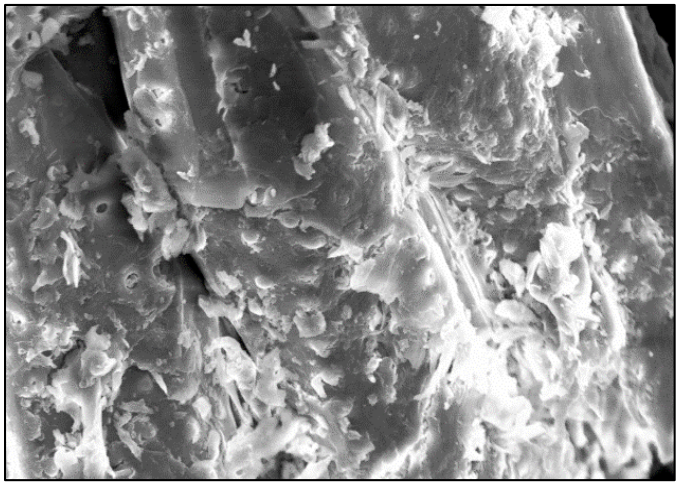

Figure 5.9 SO_4^{2-} - loaded TETS

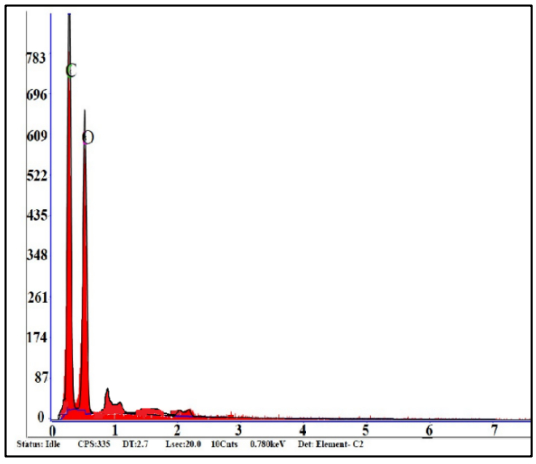

Figure 5.10 Unloaded TETS

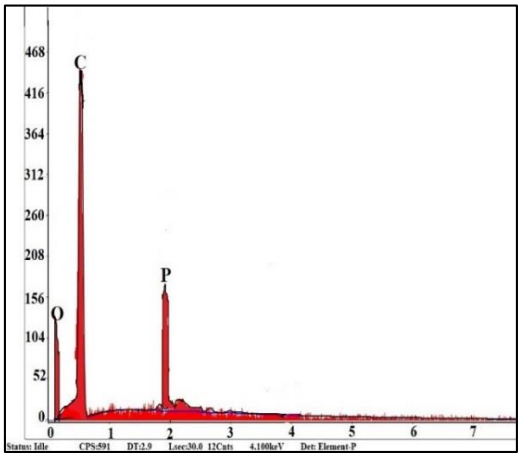

Figure 5.11 PO_4^{3-} loaded TETS

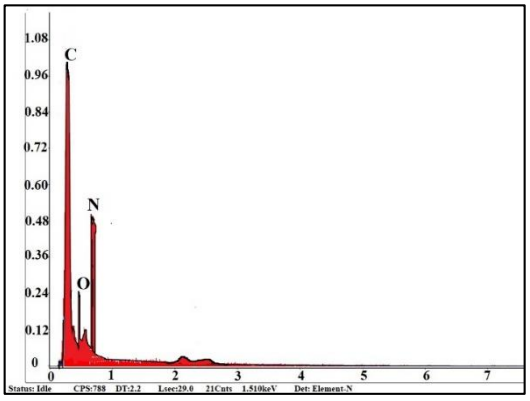

Figure 5.12 NO_3^- loaded TETS

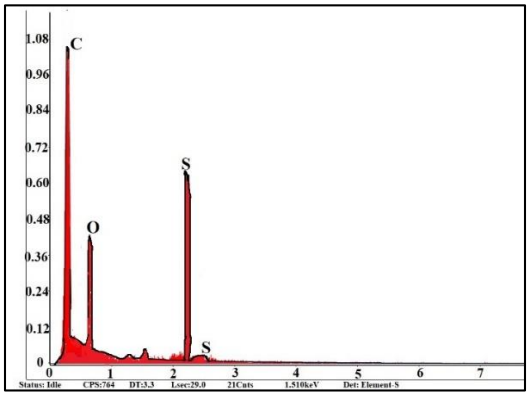

Figure 5.13 SO_4^{2-} loaded TETS

5.4 FT-IR Spectral Studies

FT-IR spectra of unloaded and anions laden TETS samples are presented in fig 5.14. Peak position at 3785 cm^{-1} indicates the stretching vibration of OH^- group, showing the presence of tannin. Peaks at 1416 cm^{-1}, 1648 $cm^{-1}$and 1037 cm^{-1} correspond to anion binding groups i.e., carbonyl and carboxyl groups[11]. Shift in wavenumber of prominent peaks and occurrence of new peaks in the spectra of anion – TETS systems imply the involvement of functional groups during adsorption process.

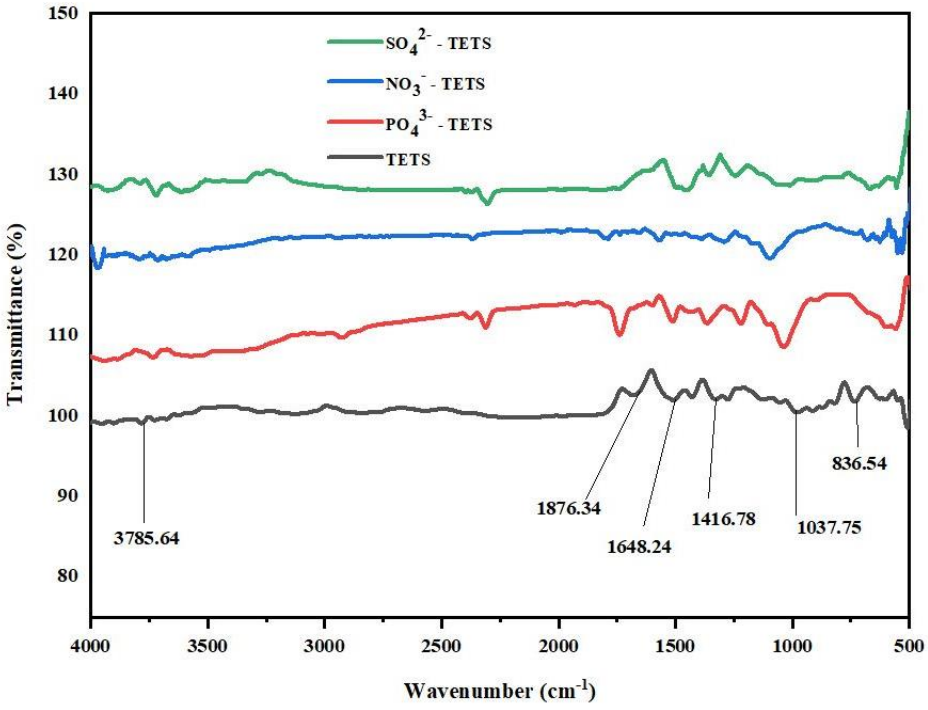

Figure 5.14 FT-IR Spectra

5.5 Batch Equilibration Experiments

5.5.1 Impact of Particle Size

Amongst the varied particle sizes of TETS experimentally verified, 0.18mm exhibited maximum sorption capacity as evident from table 5.3. Diminished particle size promotes extended surface area, which in turn lead to greater tendency to attain equilibrium in a shorter time period [12]. Thence, 0.18mm particle size is fixed as optimum size for the forthcoming experiments.

Table 5.3 Impact of Particle size

Systems	Amount adsorbed (mg/g)				
	0.18mm	**0.24mm**	**0.30mm**	**0.42mm**	**0.71mm**
PO_4^{3-} - TETS	**54.81**	45.72	38.23	29.64	22.35
NO_3^-- TETS	**48.53**	42.38	31.62	22.56	19.77
SO_4^{2-} - TETS	**51.89**	43.47	35.93	26.67	20.85

5.5.2 Impact of Initial Concentration and Agitation Time

The influences of initial anion concentrations (50 – 300 mg/L: 50 mg/L) and contact time intervals (5 - 30 mins: 5 mins) for TETS systems are illustrated in figures 5.15 – 5.17. Maximum anion adsorption at an initial concentration of 100 mg/L for PO_4^{3-}/NO_3^- and 250 mg/L for SO_4^{2-} had occurred at 5 minutes contact time, beyond which a gradual degradation is observed. This shall be attributed to the fact that, excess anions may be left unadsorbed in the solution[13].

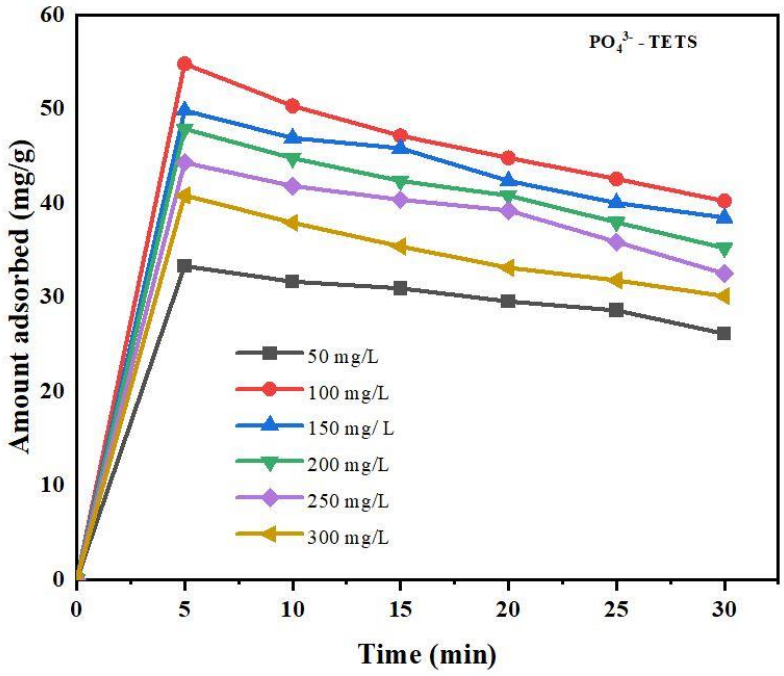

Figure 5.15 Impact of Initial Concentration and Agitation Time: PO_4^{3-}

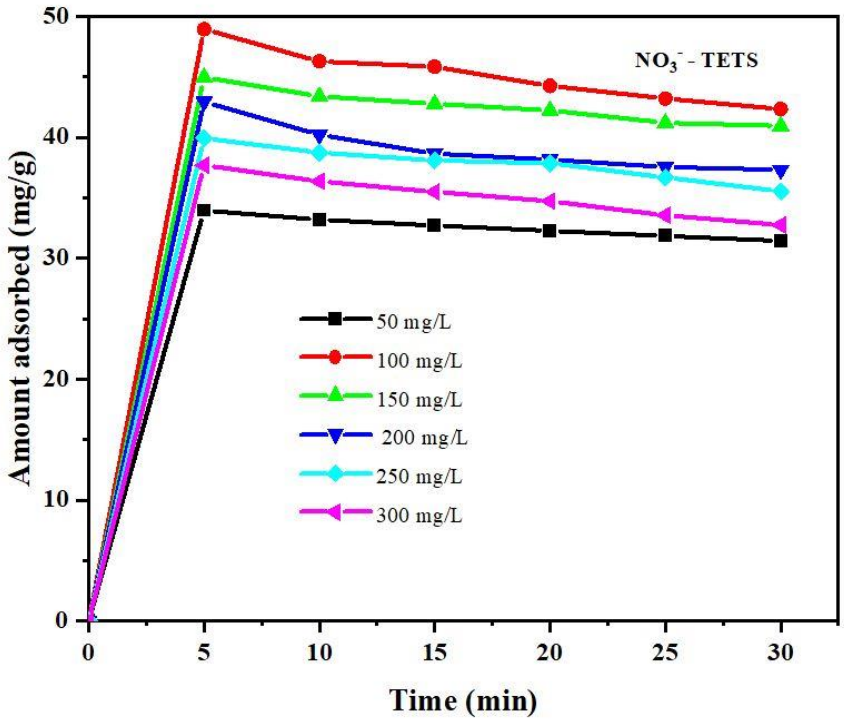

Figure 5.16 Impact of Initial Concentration and Agitation Time: NO_3^-

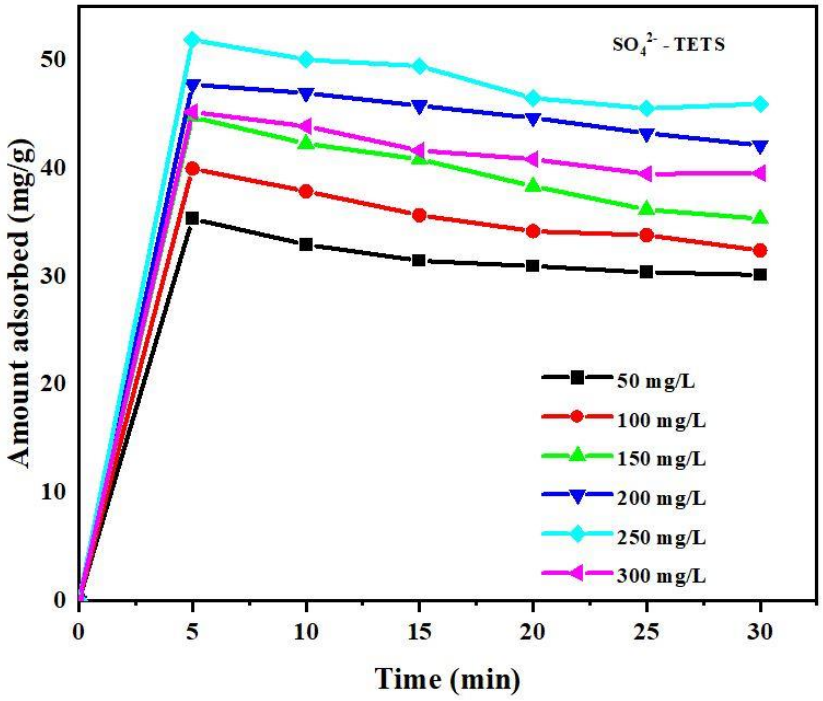

Figure 5.17 Impact of Initial Concentration and Agitation Time: SO_4^{2-}

5.5.3 Impact of Dosage

The influence of sorbent mass under optimized aforesaid parametric conditions is depicted in figure 5.18. Sorption pattern reveals that the anion percentage removal beyond the maximum begins to decline at increased sorbent dose. This may be due to the availability of greater surface area at initial stage and also, overlapping/agglomeration of adsorbent sites might have happened[14], which is supported by the inverted parabolic curves. Maximum sorption had occurred at 100 mg for PO_4^{3-} / NO_3^- and 150 mg for SO_4^{2-} respectively.

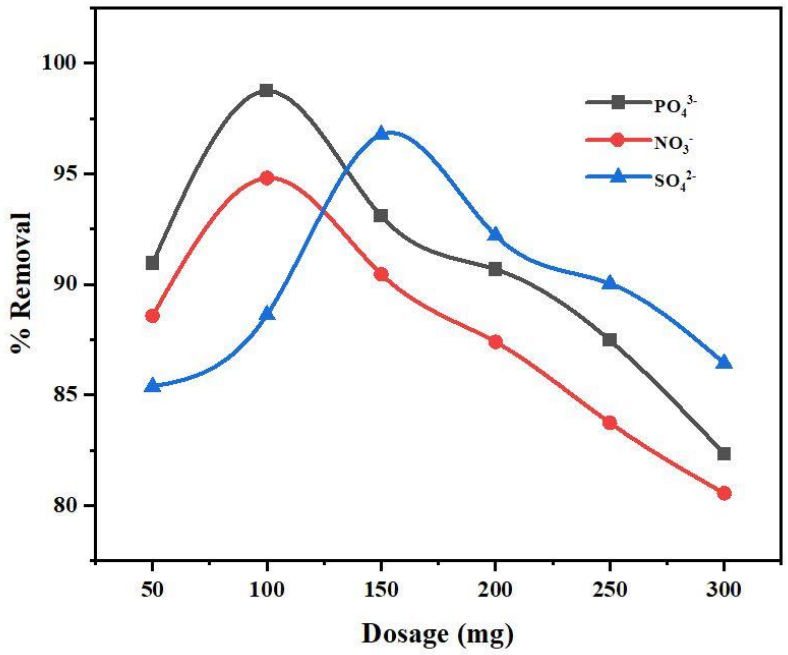

Fig: 5.18 Impact of Dosage

5.5.4 Impact of pH

pH, an important parameter shall change or control the solubility/ degree of rapid ionization of anions and concentration of counter ions being adsorbed. The sorption trend with respect to different pH environments 3 -11 reveal that ultimate percentage removal had occurred at pH 5 for the three studied systems, (table 5.4). At alkaline pH, the agitation registered a decline in the sorption process which shall be due to the operation of repulsive force between ions of similar charges.[15]

Table 5.4 Impact of pH

Systems	Percentage removal (%)				
	pH 3	pH 5	pH 7	pH 9	pH 11
PO_4^{3-} - TETS	87.6	**99.7**	82.6	78.3	69.1
NO_3^-- TETS	82.9	**97.5**	74.3	69.5	63.3
SO_4^{2-} - TETS	84.8	**98.2**	79.3	74.4	66.9

5.5.5 Impact of Ions

Selected anions adsorption by TETS being influenced by varying concentrations of specified cations /co-ions are listed in Table 5.5. The order of cation / anion inhibition viz., Mg^{2+}> Na^+., Cl^-> F^- appears to be similar as observed in chapter IV (under 4.5.5). The outer spherically sorbing Cl^- ion can moderately interfere the sorption of target anions at lower concentration than that of F^- ion (inner-spherically sorbing anion), which shows minimal interference[16].

Table 5.5 Impact of Ions

Systems	Anion removal in absence of ions	Conc. (mg/L)	Percentage Removal (%)			
			Cations		Co ions	
			Mg^{2+}	Na^+	Cl^-	F^-
PO_4^{3-} - TETS	99.7	100	**87.5**	88.3	95.2	98.1
		200	85.3	87.4	94.1	97.8
		300	84.8	85.3	93.2	96.6
		400	83.3	83.8	92.1	95.7
		500	81.8	82.6	90.8	94.8
NO_3^- - TETS	97.5	100	**83.6**	91.8	92.4	97.1
		200	82.8	90.7	90.3	96.3
		300	82.2	89.3	89.6	95.2
		400	81.7	88.6	89.2	94.5
		500	80.3	88.2	88.4	93.7
SO_4^{2-} - TETS	98.2	100	**85.6**	87.5	94.3	97.7
		200	85.3	86.5	93.8	96.3
		300	84.8	85.8	92.6	95.4
		400	83.5	84.8	92.2	94.6
		500	82.7	83.3	91.5	93.8

5.5.6 Impact of Temperature

Sorption nature of any system is dependent on the temperature factor, as the latter plays a vital role in predicting the former. Mobility of anions increases with temperature (fig 5.9), supportive of enhanced sorption rate. This shall be due to its swelling nature which is produced within the sorbent internal structure. This, in turn, favours further penetration of larger ions onto the sorbent surface[17].

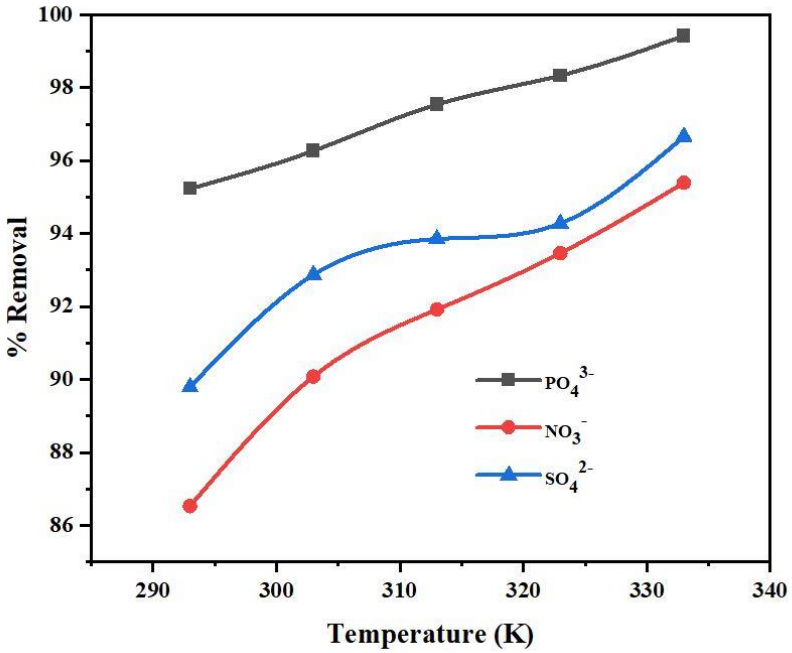

Fig: 5.19 Impact of Temperature

5.5.7 Desorption and Regeneration Studies

Desorption/regeneration studies performed, recorded a very low desorption rate, invariably for all the systems with least variations in adsorption capacity values (table 5.6). This reveals the immobilizing nature of TETS, confirming its withstanding capacity of successive use without loss of its stability / activity[18].

Table 5.6 Desorption and Regeneration Study

Systems	Cycle 1 (mg/g)		Cycle 2 (mg/g)		Cycle 3 (mg/g)	
	Adsorption	**Desorption**	**Adsorption**	**Desorption**	**Adsorption**	**Desorption**
PO_4^{3-} -TETS	52.42	1.59	44.63	1.33	39.90	1.29
NO_3^--TETS	47.74	2.53	40.84	2.76	35.34	2.84
SO_4^{2-}-TETS	50.23	3.94	42.32	3.14	37.65	3.54

5.6 Statistical Analysis

The experimental data obtained under optimized conditions were statistically approached by SPSS software and the corresponding results are listed table 5.7. Negative Pearson correlation values is obtained for almost all the parameters, suggesting inclined sorption[19]. The probability (P) values, being lesser than the significant value (0.05), indicate null hypothesis rejection for all the three systems. A favourable statistical significance is evident from F values observed to be greater than F_{crit} values based on ANOVA calculations.

Table 5.7 Statistical Data

System	Parameter	Descriptive			Pearson Correlation	P	ANOVA	
		Mean	**SD**	**SE**			**F**	**F_{crit}**
PO_4^{3-} -TETS	Particle size	14.46	1.61	0.72	-0.9334	3.21E-^{05}	373.96	5.31
	Initial anion concentration	46.83	12.03	4.91	-0.2301	0.0110	11.08	4..96
	Dosage	47.85	7.67	3.13	-0.6888	0.0127	11.01	4.96
	pH	11.61	2.41	1.08	-0.5819	-1.2286	6.70	5.31

System	Parameter	Descriptive			Pearson Correlation	P	ANOVA	
		Mean	SD	SE			F	F_{crit}
NO_3^--TETS	Particle size	11.98	1.75	0.78	-0.8823	9.11E-^{05}	214.97	5.31
	Initial anion concentration	45.47	11.80	4.81	-0.2301	0.0110	11.32	4.94
	Dosage	39.85	6.88	2.81	-0.8374	0.0103	12.45	4.96
	pH	9.49	1.89	0.84	-0.5819	0.1432	2.28	5.31
SO_4^{2-} TETS	Particle size	12.27	1.36	0.60	-0.7518	3.17E-^{05}	372.70	5.31
	Initial anion concentration	45.99	13.41	5.47	0.8946	0.0059	11.18	4.96
	Dosage	35.53	5.40	2.20	-0.3657	0.0080	13.29	4.96
	pH	10.63	1.90	0.85	-0.5034	0.0707	4.83	5.31

*E – continuous random variables

5.7 Adsorption Isotherms

Attainment of equilibrium state by PO_4^{3-}, NO_3^- and SO_4^{2-} anions at specific concentrations, in the process of registering the sorption capacity of TETS is listed in table 5.8, from which Langmuir (fig 5.20), Freundlich (fig 5.21), Temkin (fig 5.22) and DKR plots (fig 5.23) are derived. The isothermal constants, calculated from the gradients and intercepts of the studied plots and their corresponding R^2 values are listed in table 5.9.

Table 5.8 Equilibrium Concentrations- Isothermal Study

System	Anion Conc. (mg/L)	Langmuir		Freundlich		Temkin		DKR	
		C_e	C_e/q_e	log C_e	log q_e	ln C_e	q_e	ε^2*10^{-5}	ln q_e
PO_4^{3-} - TETS	50	4.25	0.27	0.62	1.19	1.44	17.55	2.83	2.74
	100	8.80	0.36	0.94	1.38	2.17	24.27	0.73	3.18
	150	14.30	0.46	1.15	1.49	2.66	30.93	0.28	3.43
	200	23.34	0.58	1.36	1.59	3.15	39.58	0.11	3.67
	250	32.83	0.74	1.51	1.64	3.49	43.94	0.05	3.78
	300	44.42	0.96	1.64	1.66	3.79	45.83	0.03	3.82
NO_3^-- TETS	50	5.28	0.45	0.72	1.06	1.66	11.52	1.90	2.44
	100	9.23	0.51	0.96	1.25	2.22	17.88	0.67	2.88
	150	19.74	0.69	1.29	1.42	2.98	28.36	0.15	3.34
	200	22.25	0.74	1.34	1.51	3.10	29.73	0.12	3.39
	250	27.53	0.82	1.43	1.54	3.31	33.32	0.08	3.50
	300	33.54	0.91	1.52	1.56	3.51	36.67	0.05	3.60
SO_4^{2-} - TETS	50	3.37	0.27	0.52	1.08	1.21	12.05	4.28	2.48
	100	9.48	0.38	0.97	1.39	2.24	24.58	0.63	3.20
	150	15.28	0.43	1.18	1.54	2.72	35.63	0.25	3.56
	200	27.84	0.64	1.44	1.63	3.32	43.36	0.07	3.76
	250	34.38	0.74	1.53	1.66	3.53	45.14	0.05	3.82
	300	48.64	0.99	1.68	1.69	3.88	48.39	0.02	3.88

Table 5.9 Isothermal Constants

Systems	Langmuir Isotherm			Freundlich Isotherm			Temkin Isotherm			DKR Isotherm		
	q_m (mg/g)	b	R^2	K_F (mg/g)	1/n	R^2	A_T (L/g)	B_T (J/mol)	R^2	q_s (mg/g)	E (KJ/mol)	R^2
PO_4^{3-} - TETS	**63.69**	0.07	0.9977	8.41	2.12	0.9261	0.02	182.82	0.9115	39.72	1.08	0.9423
NO_3^-- TETS	**59.17**	0.04	0.9984	4.11	1.56	0.9026	0.05	158.07	0.8995	32.67	1.29	0.9198
SO_4^{2-} - TETS	**60.97**	0.07	0.9956	7.01	1.87	0.9177	0.03	174.22	0.9087	41.41	1.18	0.9235

5.7.1 Langmuir Model

Linearity of Langmuir plot and the calculated R_L values (Table 5.9) being < 1 favour the applicability of the model for TETS systems pertaining to the three anions. This is also supported by the adsorption capacity q_m values which exhibits coherency with the experimentally derived q_e values, thereby favouring monolayer adsorption.

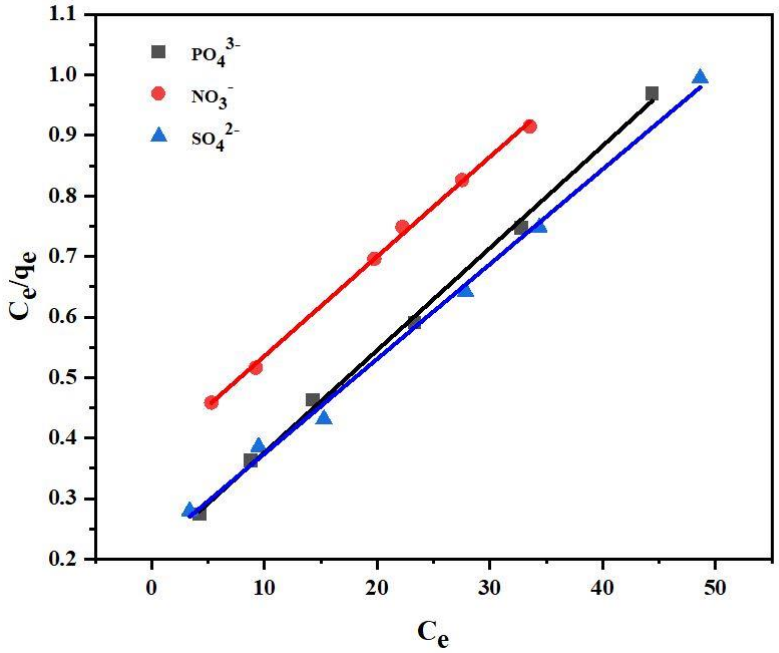

Figure 5.20 Langmuir Plot

Table 5.10 Equilibrium Parameter (R_L)

Conc. mg/L	PO_4^{3-} - TETS	NO_3^--TETS	SO_4^{2-} - TETS
50	0.22	0.33	0.22
100	0.12	0.20	0.12
150	0.08	0.14	0.08
200	0.06	0.11	0.06
250	0.05	0.09	0.05
300	0.04	0.07	0.04

5.7.2 Freundlich Model

Prominent deviation from the linear nature of the values plotted reveal lesser fit of Freundlich model to TETS systems. A significant variation in these q_e, K_F, R^2 values plot is quiet obvious while comparing with Langmuir implying the occurrence of preferential adsorption as monolayer instead of multilayer.

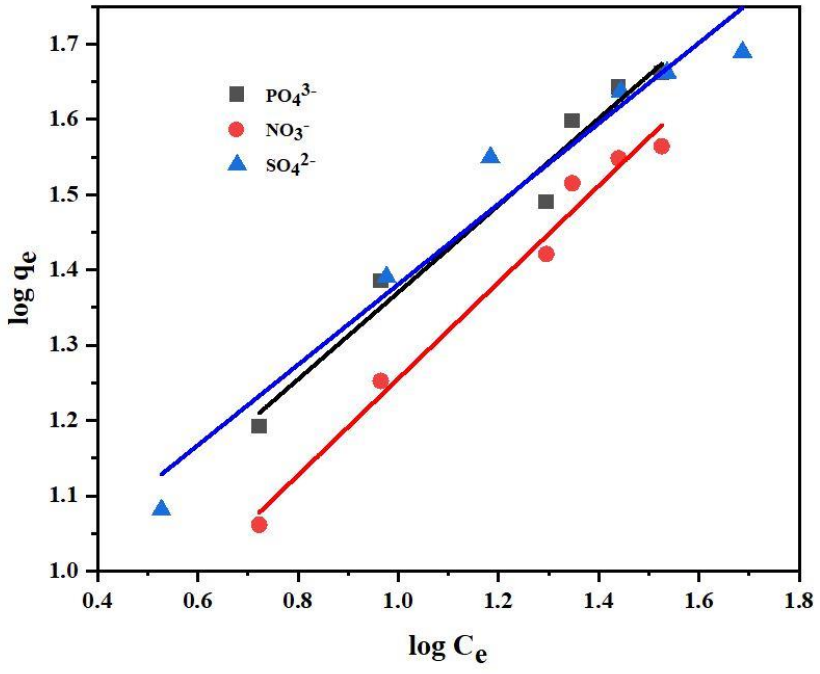

Figure 5.21 Freundlich Plot

5.7.3 Temkin Model

Lower A_T values indicative of binding constant and higher B_T value, registering greater heats of adsorption denote the non-applicability of the model[21]. Also, valid deviations of points from the straight line (fig 5.21) show R^2 values to be around 0.9000 only.

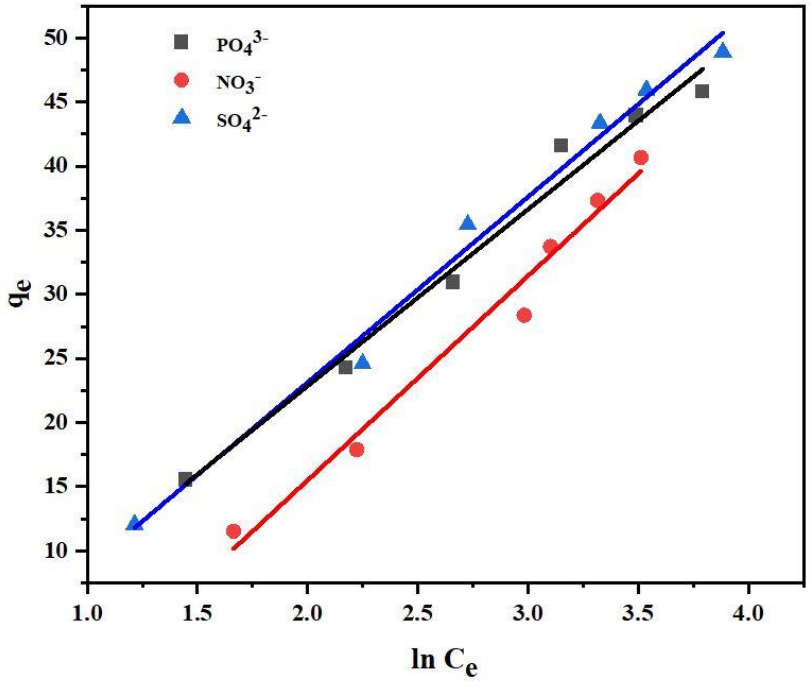

Figure 5.22 Temkin Plot

5.7.4 Dubinin– Kaganer -Radushkevich Model

Mean sorption energy value (E) are expected to be greater than 8 kJ/ mol in chemisorption mode.[22,23] The recorded E values (1.08, 1.29, 1.18 for the three systems) are lower than the stated value, foothold that the systems follow physisorption only [24]. This is in favour with the applicability of Langmuir model as mentioned in 5.7.1.

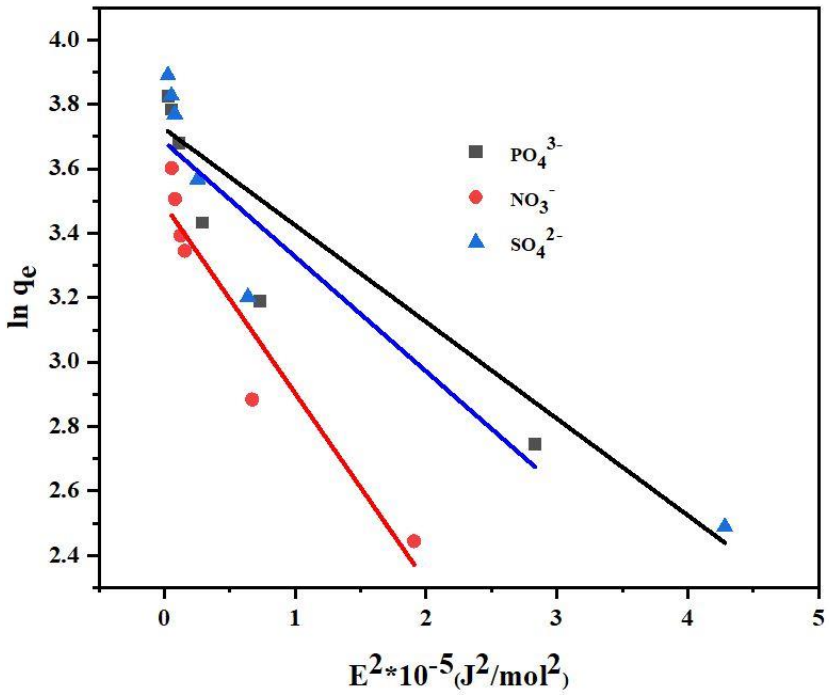

Figure 5.23 DKR Plot

5.7.5 Comparison of Isotherm Models

Calculated adsorption capacity values for TETS, wherein, $q_m > K_F$, q_s infer the best suitability of Langmuir model for all the anions. Correlation coefficient values (R^2) observed from the respective graphs, register the following pattern: Langmuir > DKR > Freundlich > Temkin.

5.8 Adsorption Kinetics

Kinetic studies predict the progress of adsorption. However, determination of adsorption mechanism is important for design purposes. In this view, four kinetic models are discussed for TETS systems as done in chapter IV.

5.8.1 Pseudo First Order/ Pseudo Second Order Models

Experimental data corresponding to pseudo models for the studied systems are represented in table 5.11 and their relative linear plots are shown in figures 5.24 & 5.25. Rate constants (q_{cal}, K_1, K_2), along with R^2 values inferred from the slopes and intercepts

of respective graphs are stated in table 5.12. A relatively higher correlation coefficient values is evident from the table, favouring the applicability of pseudo second order kinetic model, thus facilitating the better description of the adsorption systems by this model.

Table 5.11 Pseudo Models – Data

Time (min)	PO_4^{3-} - TETS			NO_3^-- TETS			SO_4^{2-} - TETS		
	log (qe-qt)	qt	t/qt	log (qe-qt)	qt	t/qt	log (qe-qt)	qt	t/qt
5	1.76	43.25	0.10	1.83	30.58	0.14	2.32	28.46	0.11
10	1.74	44.82	0.20	1.83	31.64	0.29	2.32	29.72	0.23
15	1.73	45.73	0.32	1.83	32.33	0.44	2.32	30.66	0.35
20	1.72	46.58	0.43	1.82	33.75	0.61	2.31	31.98	0.49
25	1.71	47.64	0.55	1.81	34.48	0.79	2.31	32.47	0.62
30	1.70	48.92	0.69	1.81	35.32	0.98	2.31	33.59	0.75

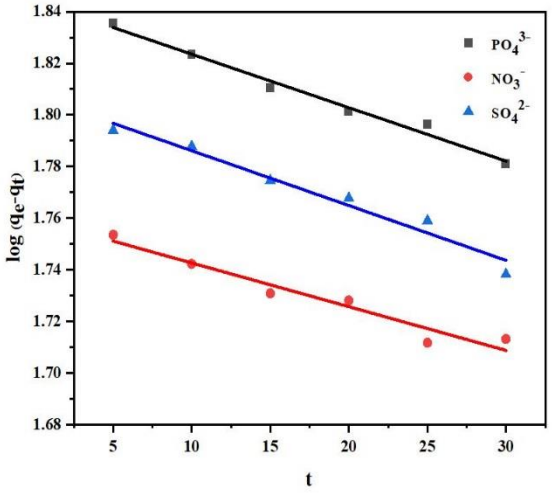

Figure 5.24 Pseudo First Order Kinetics

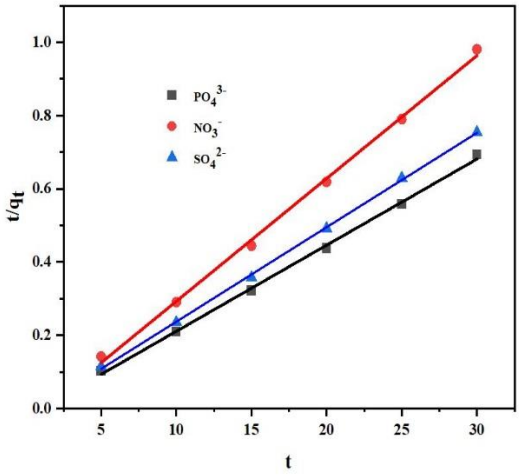

Figure 5.25 Pseudo Second Order Kinetics

Table 5.12 Pseudo First Order/ Pseudo-Second Order Parametric values

Conc. of Anions (mg/L)	q_{exp} (mg/g)	Pseudo First Order				Pseudo Second Order			
		$q_{cal.}$ (mg/g)	$k_1 \times 10^{-3}$ (min^{-1})	R^2	SSE	$q_{cal.}$ (mg/g)	$K_2 \times 10^{-3}$ (min^{-1})	R^2	SSE
PO_4^{3-} - TETS									
50	42.32	10.32	0.45	0.9362	12.00	48.78	0.19	0.9993	7.23
100	**60.81**	59.62	0.53	0.9578	24.81	**52.55**	0.22	0.9984	1.13
150	49.84	109.92	0.13	0.9358	53.08	45.24	0.26	0.9987	5.80
200	47.89	162.74	0.69	0.9071	57.42	43.98	0.34	0.9996	3.45
250	44.31	217.17	0.69	0.9357	88.43	39.91	0.21	0.9993	0.70
300	40.83	273.14	0.92	0.9389	118.42	37.08	0.15	0.9962	0.87
NO_3^- - TETS									
50	35.94	19.05	0.64	0.9213	6.19	40.25	0.20	0.9996	4.41
100	**55.93**	69.75	0.25	0.9499	13.41	**46.76**	0.26	0.9980	1.58
150	44.95	120.94	0.11	0.9358	33.09	43.67	0.31	0.9977	5.54
200	42.93	175.26	0.11	0.9158	63.16	41.06	0.11	0.9991	3.93
250	39.91	230.30	0.09	0.9297	95.19	36.95	0.16	0.9964	1.48
300	37.68	284.24	0.04	0.9065	124.28	32.05	0.23	0.9968	2.31
SO_4^{2-} - TETS									
50	35.34	11.23	0.23	0.9446	13.07	39.66	0.21	0.9986	4.14
100	39.96	63.12	0.23	0.9363	14.15	41.84	0.27	0.9993	3.51
150	44.75	117.92	0.16	0.9127	37.27	42.61	0.21	0.9990	2.38
200	47.13	172.30	0.11	0.9012	59.08	44.96	0.16	0.9976	4.58
250	**57.89**	211.78	0.09	0.9407	75.94	**49.75**	0.31	0.9994	0.57
300	45.21	273.96	0.04	0.9289	106.87	40.21	0.28	0.9998	2.00

5.8.2 Elovich Model

Elovich constants α, β (Table 5.13) referring to initial sorption rate and extent of surface coverage respectively were calculated from the intercepts and slopes of Elovich plot (fig 5.25). α values follow decreasing order at increasing anion concentrations, whereas β values are directly linked to the concentration range, thereby confirming enhancement in the extent of surface coverage by anionic species[25].

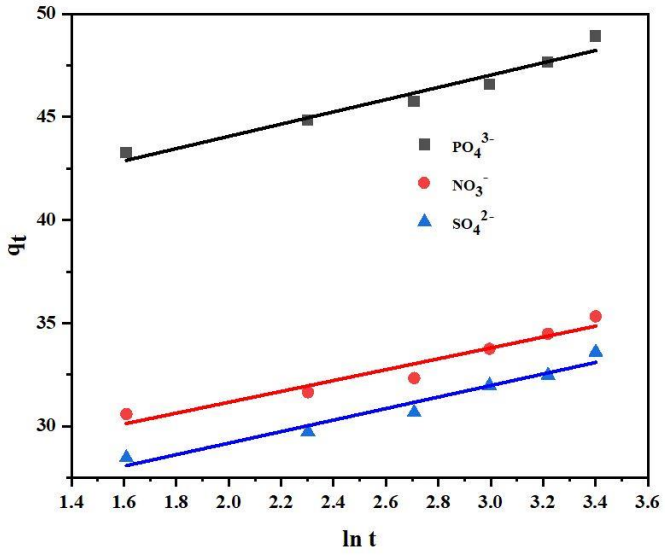

Figure 5.26 Elovich Plot

Table 5.13 Elovich Constants

Conc. (mg/L)	PO_4^{3-} - TETS			NO_3^--TETS			SO_4^{2-} - TETS		
	α	β	R^2	α	β	R^2	α	β	R^2
50	39.57	1.85	0.9595	32.27	1.43	0.9010	36.16	1.60	0.9035
100	37.10	1.97	0.9506	25.88	1.68	0.9375	34.17	1.88	0.9205
150	36.36	2.34	0.8786	26.10	1.96	0.9312	29.21	2.17	0.9573
200	34.55	2.63	0.9360	20.99	2.15	0.9433	27.14	2.50	0.9404
250	28.93	2.82	0.9171	15.24	2.59	0.8974	23.88	2.79	0.9588
300	23.72	2.97	0.8740	13.39	2.72	0.8650	23.37	2.83	0.9336

5.8.3 Intraparticle Diffusion Model

Values of intraparticle diffusion constants, viz., K_{id} and C mentioned in table 5.14, were calculated from the slopes and intercepts of the plot (q_t vs $t^{1/2}$) illustrated in figure 5.26. A steep rise in the curves, followed by deviation near saturation might be due to the diffusion occurring between the mass transfer rate in the initial and final stages of the sorption[26]. This affirms that surface sorption and intra particle diffusion are operating concurrently during the interactions between sorbent – sorbate species[27].

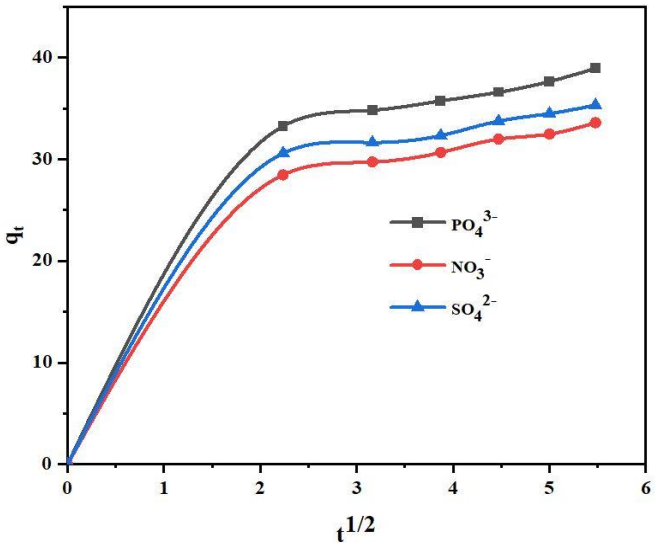

Figure 5.27 Intraparticle Diffusion Plot

Table 5.14 Intraparticle Diffusion Constants

Conc. (mg/L)	PO_4^{3-} - TETS		NO_3^-- TETS		SO_4^{2-} - TETS	
	K_{id}	C	K_{id}	C	K_{id}	C
50	1.53	24.78	1.41	14.11	1.49	20.41
100	1.66	30.26	1.58	16.55	1.56	24.42
150	2.96	35.02	1.87	22.19	1.65	29.39
200	2.98	38.55	2.41	27.08	2.23	34.98
250	3.37	39.41	2.61	30.05	2.56	37.12
300	3.54	42.63	3.04	36.59	3.31	40.76

5.8.4 Comparison of Kinetic Models

Experimentally determined and calculated q_e values are in good agreement in case of Pseudo second order model against Pseudo first order. Consideration of correlation coefficients / SSE values favour the above statement, describing the better fit of Pseudo second order kinetic model for TETS systems, amongst other studied models.

5.9 Adsorption Dynamics

Sorption dynamics were investigated at under different temperatures. Van't Hoff's plot, ln K_c vs 1/T (fig 5.28), the negative values of $\Delta G°$ at increasing temperatures denotes spontaneous nature of sorption. The positive values of $\Delta H°$ and $\Delta S°$ (Table 5.15) suggest the adsorption process to be endothermic with elevated randomness of the solid liquid interface during agitation[28,29].

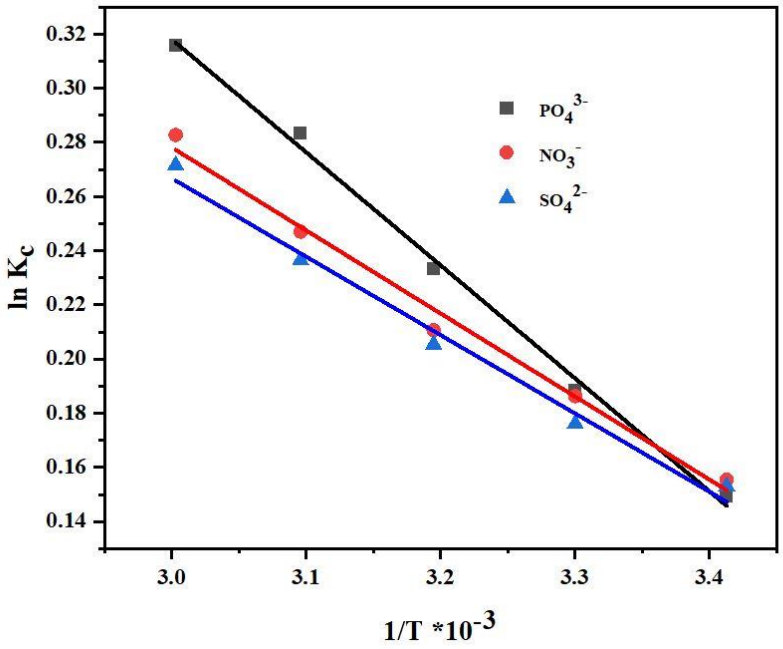

Figure 5.28 Van't Hoff's Plot

Table 5.15 Thermodynamic Constants

Temp. (K)	PO_4^{3-} - TETS			NO_3^--TETS			SO_4^{2-} TETS		
	$\Delta G°x10^{-3}$ kJ/ mol	**$\Delta H°$ kJ/ mol**	**$\Delta S°$ kJ/ mol**	**$\Delta G°x10^{-3}$ kJ/ mol**	**$\Delta H°$ kJ/ mol**	**$\Delta S°$ kJ/ mol**	**$\Delta G°x10^{-3}$ kJ/ mol**	**$\Delta H°$ kJ/ mol**	**$\Delta S°$ kJ/ mol**
293	-0.39	3.46	13.04	-0.35	2.40	9.43	-0.37	2.54	9.79
303	-0.47			-0.44			-0.46		
313	-0.60			-0.53			-0.55		
323	-0.76			-0.63			-0.67		
333	-0.87			-0.74			-0.79		

5.10 References

[1] T. K. Naiya, A. K. Bhattacharya, S. Mandal and S. K. Das, The Sorption of Lead (II) Ions on Rice Husk Ash, *Journal of Hazardous Materials,* 163 **(2009)** 1254-1264

[2] V. P. Della, I. Kuhn and D. Hotza, Characterization of Rice Husk Ash for use as Feedstock in the Manufacture of Silica Refractories, *Quimica Nova*, 24 **(2001)** 778-782

[3] V. C. Srivastava, I. D. Mall and I. M. Mishra, Characterization of Mesoporous Rice Husk Ash (RHA) and Adsorption Kinetics of Metal Ions from Aqueous Solution onto RHA. *Journal of Hazardous Materials,* 134 **(2006)** 257-267

[5] P. Sirisomboona, P. Kitchaiyab, T. Pholphoa, W. Mahuttanyavanitcha Physical and Mechanical properties of *Jatropha curcas* L. fruits, nuts and kernels, *Biosystems Engineering,* 97 **(2007)** 201– 207

[6] Charles Emeka Osakwe, Isma'il Sanni, Suraj Sa'id and Adamu Zubairu, Adsorption of Heavy Metals from Wastewaters using *Adonosia digitata* Fruit Shells and *Theobroma cacao* Pods as Adsorbents: A Comparative Study, *AU Journal of Technology,* 18(1) **(2014)**11-18

[7] Adie D.B Okuofu C.A. Osakwe C., Comparative Analysis of the Adsorption of Heavy Metals in Wastewater Using Borrassus Aethiopium and Cocos Nucifera, *International Journal of Applied Science and Technology,* 2 (7) **(2012)**

[8] Nasiru Abdus and Magaji Buhari, Adsorption of Alizarin and Fluorescein Dyes on Adsorbent prepared from Mango Seed, *Pac. Journal of Science Technology,* 15(1) **(2014)** 232-244

[9] P.S. Kumar, S.Ramalingam, S.D. Kirupha, A. Murugesan, T. Vidyadevii, S. Sivanesan, Adsorption Behaviour of Nickel(II) onto Cashew nut shell: equilibrium, thermodynamic, mechanism and process design, *Chemical Engineering Journal,*167 **(2011)** 122-131

[9] Chen Yunnen, Wu Ye, Liu Chen, Guo Lin, Nie Jinxia, Ren Rushan, Continuous fixed-bed column study and adsorption modeling: Removal of Arsenate and Arsenite in aqueous solution by organic modified Spent grains, *Pol. J. Environ. Stud,* 4 **(2017)** 1847-1854

[10] Ari Clecius A. de Limaa,1, Ronaldo F. Nascimentoa,1, Francisco F. de Sousa b,2, Josue M. Filho b,2, Alcineia C. Oliveiraa, Modified coconut shell fibers: A green and economical sorbent for the removal of anions from aqueous solutions, *Chemical Engineering Journal,* 185-186 **(2012)** 274 - 284

[12] Marcus. Y, *Ion Properties, CRC Press,* New York, 272 **(1997)**

[13] G. McKay, H. S. Blair, J. R. Gardner, Adsorption of dyes on chitin. I. Equilibrium studies, *Journal of Applied Polymer Science,* 27 **(1982)** 3043 – 3057

[4] Wimonrat Tongpoothorn, Manop Sriuttha, Phunsiri Homchan, Saksit Chanthai, Chalerm Ruangviriyachai, Preparation of Activated Carbon derived from *Jatropha curcas* fruit shell by Simple Thermo-chemical Activation and Characterization of their Physico-chemical properties, *Chemical Engineering Research and Design,* 8 (9) **(2011)** 335–340

[14] Mustafa Gazi, Akeem Adeyemi Oladipo & Kola A. Azalok, Highly Efficient and Magnetically Separable Palm seed-based Biochar for the removal of Nickel, *Separation Science and Technology,* **(2017)** 1 - 28

[15] M Suneetha1 and K Ravindhranath, Removal of Nitrates from Polluted Waters using Bio-Adsorbents, *International Journal of Life Sciences Biotechnology and Pharma Research,* 3 **(2012)** 151 - 160

[16] Salah H Aljbour, Adnan M Al-Harahsheh and Mohammad A Aliedeh, Phosphate Removal from Aqueous Solutions by using natural Jordanian zeolitic tuff, *Adsorption Science and Technology,* 0 **(2016)** 1 -16

[17] Chinnaiya Namasivayam, Molagoundampalayam and V. Sureshkumar, Removal of Sulfate from Water and Wastewater by Surfactant Modified Coir Pith, an Agricultural Solid Waste by Adsorption Methodology, *Journal of Environmental Engineering Management,* 17 **(2007)** 129 -135

[19] Edmund C. Okoroigwe, Christopher M. Saffron, Pascal D. Kamdem, Characterization of Palm Kernel Shell for Materials reinforcement and Water Treatment, *Journal of Chemical Engineering and Materials Science*, 5(1) **(2014)** 1-6

[20] Ilango Aswin Kumar, Narayasamy Viswanathan, A Facile Synthesis of Magnetic Particles Sprayed Gelatin Embedded Hydrotalcite Composite for Effective Phosphate Sorption, *Journal of Environmental Chemical Engineering*, 6 **(2018)** 208 - 217

[21] P.Nammalvar, Natioanl Symposium on Eutuarian Management, Trivandrum Proceedings, **(1985)**, 235- 238

[22] Ahmet Örnek, Mahmut Özacar, İ. Ayhan Şengil, Adsorption of lead onto formaldehyde or sulphuric acid treated acorn waste: Equilibrium and kinetic studies, *Biochemical Engineering Journal,* 37 **(2007)** 192–200

[23] B.M.W.P.K. Amarasinghe, R.A. Williams, Tea waste as a low cost adsorbent for the removal of Cu and Pb from wastewater, *Chemical Engineering Journal*, 132 **(2007)** 299–309

[24] Sharda Gupta, Dhananjay Kumar, J.P. Gaur, Kinetic and isotherm modeling of lead(II) sorption onto some waste plant materials, *Chemical Engineering Journal*, 148 **(2009)** 226–233

[25] V. K. Gupta and A. Rastogi, Biosorption of Lead from Aqueous Solutions by Green Algae Spirogyra species: Kinetics and Equilibrium studies, *Journal of Hazardous Materials*, 152 **(2008)** 407-414

[26] Ting Fan, Yunguo Liu, Baoying Feng, Guangming Zeng, Chunping Yang, Ming Zhou, Haizhou Zhou, Zhenfeng Tan, Xin Wang, Biosorption of Cadmium(II), Zinc(II) and Lead(II) by Penicillium simplicissimum: Isotherms, Kinetics and Thermodynamics, *Journal of Hazardous Materials,* 160 **(2008)** 655-661

[27] Suresh Gupta, B.V. Babu, Utilization of Waste Product (tamarind seeds) for the Removal of Cr(VI) from Aqueous Solutions: Equilibrium, Kinetics and Regeneration studies, *Journal of Environmental Management*, 90 **(2009)** 3013-3022

[28] V. C. Srivastava, I. D. Mall and I. M. Mishra, Characterization of Mesoporous Rice Husk Ash (RHA) and Adsorption Kinetics of Metal Ions from Aqueous Solution onto RHA. *Journal of Hazardous Materials,* 134 **(2006)** 257-267

[29] Mehmet Emin Argun, Sukru Dursun, Celalettin Ozdemir, Mustafa Karatas, Heavy Metal Adsorption by Modified Oak Sawdust: Thermodynamics and Kinetics, *Journal of Hazardous Materials,* 141 **(2007)** 77-85.